Available online at www.sciencedirect.com

ScienceDirect

Energy Procedia 63 (2014) 5631 – 5645

Energy Procedia

GHGT-12

Phase Behaviour of CO_2–Brine and CO_2–Oil Systems for CO_2 Storage and Enhanced Oil Recovery: Experimental Studies

Nader Mosavat[a], Ali Abedini[a], Farshid Torabi[a]*

[a]*Petroleum Systems Engineering, Faculty of Engineering and Applied Science, University of Regina*
3737 Wascana Parkway, Regina,SK S4S 0A2, Canada

Abstract

This study was conducted to investigate the phase behaviour of CO_2–brine and CO_2–oil systems under various operating conditions. Through this study, CO_2 solubility measurement tests were carried out for CO_2–water, CO_2–brine, and CO_2–oil mixtures at various equilibrium pressures ranging P_{eq} = 0.7–10.3 MPa and temperatures ranging T_{exp} = 21–40 °C. Additionally, series of oil swelling/extraction tests were conducted at aforementioned experimental conditions using a see-through high-pressure cell to determine the oil swelling factor at various equilibrium conditions. CO_2 solubility measurement tests showed that at constant temperatures, an increase in CO_2 solubility value was observed for CO_2–water, CO_2–brine, and CO_2–oil mixtures when the equilibrium pressure increases. Furthermore, as it was expected for all mixtures, the solubility of CO_2 reduces with increased temperature. In this study, it was also found that at a constant temperature, the oil swelling factor, *SF*, increases up to a pressure so called extraction pressure, P_{ext}, at which majority of the light to medium hydrocarbon groups in the oil phase are extracted by CO_2 and vaporized into the CO_2-rich phase. Additionally, it was observed that for the pressures higher than the extraction pressure, the oil swelling factor reduced with equilibrium pressure because more hydrocarbon components were extracted at higher pressures. The extraction pressure was determined at different experimental temperatures and results revealed that the extraction pressure increases by increasing experimental temperature. Comparison of the CO_2 solubility values in oil at extraction pressures corresponding to different experimental temperatures also showed that the major hydrocarbon extraction occurs when a certain amount of CO_2 has dissolved in the oil phase which is called threshold CO_2 solubility, χ_{th}. The defined threshold CO_2 solubility was found to be approximately the same for the CO_2–oil mixture under this study at different temperatures.

Peer-review under responsibility of the Organizing Committee of GHGT-12

Keywords: CO_2 solubility; Oil swelling factor; Light hydrocarbon extraction; Phase behaviour; CO_2-based EOR; CO_2 storage.

* Corresponding author. Tel.: +1-306-585-5667; fax: +1-306-585-4855.
E-mail address: farshid.torabi@uregina.ca

Peer-review under responsibility of the Organizing Committee of GHGT-12
doi:10.1016/j.egypro.2014.11.596

1. Introduction

Knowledge of the physical and chemical properties of CO_2, brine, and oil as well as the interactions between them in binary or ternary systems (i.e., CO_2–brine, CO_2–oil, and CO_2–brine–oil systems) together with their effects on oil recovery and CO_2 storage capacity are very crucial for any CO_2-based EOR and carbon capture and storage (CCS) projects. One of the major parameters that remarkably affect the performance of the EOR processes is the CO_2 solubility in the oil phase because it results in oil viscosity reduction and swelling, which consequently, enhances the oil recovery [1–3]. Moreover, one of the main trapping mechanisms that involves in the process of storing CO_2 in deep saline aquifers is solubility trapping and most of the injected CO_2 is trapped through dissolving in the formation brine [4–6]. Therefore, a better understanding of solubility and its effects on oil recovery and CO_2 storage mechanisms is essential and plays important role in the success of CO_2-based EOR and CO_2 storage projects.

The CO_2 solubility in the brine or oil phase and its influences on the brine or oil physical properties can be determined by experimental studies and available modelling packages or correlations. However, the available models can only be used in the limited situations, and hence, may not be applicable in wide range of operating conditions, particularly for CO_2-based EOR and CO_2 storage processes. Physical fluid properties including brine density and viscosity, CO_2 solubility in brine, oil viscosity and density, CO_2 solubility in oil, and oil swelling factor are the key parameters required to design and simulate the oil recovery and CO_2 storage processes [7–11].

The solubility of CO_2 in pure water and brines has been studied by various researchers [12–18]. Other studies showed that pressure, temperature, and salinity are the most important parameters affecting the CO_2 solubility in brine [19–24]. In addition to previously conducted experimental studies, there exist some proposed thermodynamic models to predict the CO_2 solubility values in pure water and brine [25–27]. Although literatures provide a good database for CO_2 solubility in pure water and brine, more reliable experimental data is required specially in the range of operating conditions suitable for CO_2 storage scenarios.

CO_2 solubility in crude oil is a function of several thermodynamic parameters mainly saturation pressure, temperature, and crude oil properties [7–10, 28]. Several mathematical correlations have also been developed to estimate the CO_2 solubility in crude oil. However, such correlations are accurate in particular ranges of operating conditions and fluid properties. Therefore, detailed investigations of CO_2 solubility in crude oil and oil swelling factor as a result of CO_2 dissolution are required to thoroughly distinguish the important mechanisms associated with CO_2-based EOR techniques.

The main objective of this study is to investigate the phase behaviour of various CO_2-saturated systems including CO_2–water, CO_2–brine, and CO_2–oil systems. This was accomplished through conducting series of CO_2 solubility measurement tests in pure water, brine, and crude oil. Impacts of various operating parameters (i.e., pressure and temperature) as well as brine salinity on CO_2 solubility in pure water and brine were determined. Furthermore, series of solubility and swelling/extraction tests were implemented under desired operating conditions in order to examine the CO_2 solubility in the oil phase and oil swelling factor, respectively. In addition a comprehensive interpretation was conducted on swelling/extraction curves at various temperatures to recognize the details of the mutual interactions in CO_2–oil system.

Nomenclature

Symbols

m_{dis}	Mass of CO_2 dissolved in the oil (gr)
MW_o	Oil molecular weight (gr/mole)
P_{atm}	Atmospheric pressure (101.1 kPa)
P_{eq}	Equilibrium pressure (MPa)
P_f	Final pressure (MPa)
P_i	Initial pressure (MPa)
P_{liq}	Liquefaction pressure (MPa)
P_{max}	Maximum operating pressure (MPa)
R	Universal gas constant (8.314 J/mol.K)
s	Brine salinity (mole/kg)

SF_{max}	Maximum oil swelling factor
T_{exp}	Experimental temperature (°C)
$V_{CO2,f}$	Final CO_2 volume (cm^3)
$V_{CO2,i}$	Initial CO_2 volume (cm^3)
$V_{o,f}$	Final oil volume (cm^3)
$V_{o,i}$	Initial oil volume (cm^3)
Z	Gas compressibility factor
Greeks	
μ_b	Water viscosity (mPa.s)
μ_o	Oil viscosity (mPa.s)
ρ_b	Brine density (kg/m^3)
ρ_o	Oil density (kg/m^3)
χ_b	CO_2 solubility in brine (mole CO_2/kg brine)
χ_o	CO_2 solubility in oil (gr CO_2/100 gr oil)
$\chi_{o,max}$	CO_2 solubility in oil phase at extraction pressure (gr CO_2/100 gr oil)
χ_{th}	Threshold CO_2 solubility in oil (gr CO_2/100 gr oil)
χ_w	CO_2 solubility in pure water (mole CO_2/kg water)
Abbreviations	
BPR	Back pressure regulator
CCS	Carbon capture and storage
EOR	Enhanced oil recovery
GC	Gas Chromatography
GWR	Gas to water ratio
PVT	Pressure, volume, and temperature
SF	Swelling factor

2. Materials

The CO_2 used in this study was sourced from a high purity CO_2 cylinder (99.99%, Praxair Co.). Synthetic brine of 20,000 ppm NaCl was prepared using deionized water. The density and viscosity of the brine were measured to be ρ_b = 1010.2 kg/m^3 and μ_b = 0.90 mPa.s, respectively at the temperature of T_{exp} = 25 °C and atmospheric pressure (i.e., Patm = 101.1 kPa). The physical properties of the brine and CO_2 used in the experiments carried out in this study are shown in Table 1. A DV-II+Viscometer (Can-AM Instruments LTD.) was also used to measure brine viscosity at different temperatures of T_{exp} = 25 °C and 40 °C. The light stock tank oil sample under study was a mixture of few samples taken from Bakken formation in Saskatchewan, Canada. The hydrocarbon group compositional analyses and the carbon number distribution of the oil sample are presented in Table 2 and Figure 1, respectively.

Table 1. The physical properties of the brine sample and CO_2 used in this study at atmospheric pressure (i.e., P_{atm} = 101.3 MPa) and two temperatures of T_{exp} = 25 °C and 40 °C.

Fluid	Density (kg/cm^3) P_{atm}, 25 °C	Density (kg/cm^3) P_{atm}, 40 °C	Viscosity (mPa.s) P_{atm}, 25 °C	Viscosity (mPa.s) P_{atm}, 40 °C
Brine	1010.2	1008.2	0.90	0.70
CO_2	1.8093	1.7205	0.0149	0.0156

Table 2. Compositional Analysis of the light crude oil sample under study at Texp = 21°C and atmospheric pressure.

Carbon number	Mole %	Carbon number	Mole %	Carbon number(s)	Mole %
C_1	0	C_{12}	4.48	C_{28}	0.44
C_2	1.58	C_{13}	4.02	C^{29}	0.33
C_3	0.92	C_{14}	3.32	C_{30+}	2.85
i-C_4	0	C_{15}	3.06		
n-C_4	3.88	C_{16}	2.37	C_1–C_6	22.48
i-C_5	2.20	C_{17}	2.06	C_{7+}	77.52
n-C_5	4.03	C_{18}	1.91		
C_5	0.49	C_{19}	1.51	C_1–C_{14}	78.82
i-C_6	3.07	C_{20}	1.29	C_{15+}	21.18
n-C_6	2.95	C_{21}	1.29		
C_6	3.37	C_{22}	0.76	C_1–C_{29}	97.15
C_7	13.87	C_{23}	0.87	C_{30+}	2.85
C_8	10.46	C_{24}	0.71		
C_9	8.19	C_{25}	0.66		
C_{10}	6.38	C_{26}	0.57		
C_{11}	5.61	C_{27}	0.49		

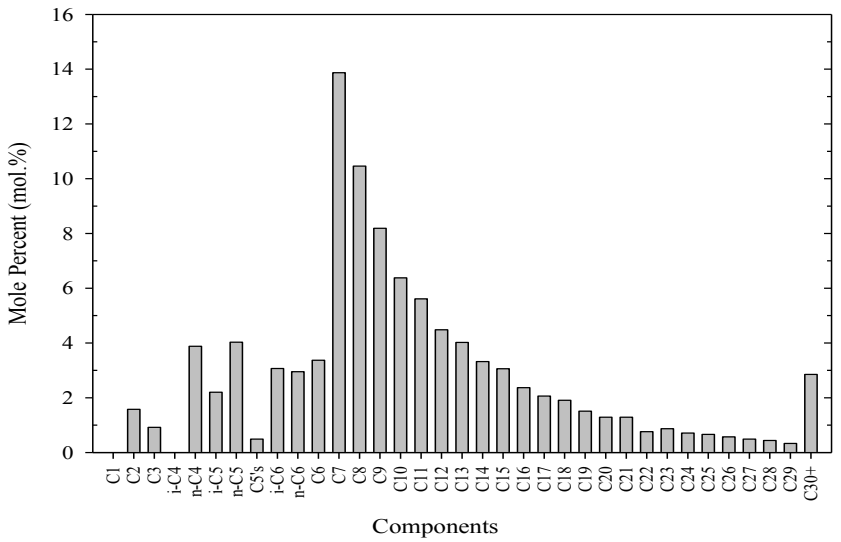

Figure 1. Results of gas chromatography (GC) compositional analysis for the mixture of Bakken crude oil samples used in this study.

Density and viscosity of the crude oil sample were ρ_o = 799.0 kg/m^3 and μ_o = 2.76 mPa.s at the temperature of T_{exp} = 25 °C and atmospheric pressure of P_{atm} = 101.1 kPa. The asphaltene content (n-Pentane insoluble) of the crude oil sample was also measured to be w_{asph} = 1.23 wt.%. Table 3 summarizes different characteristics of crude oil sample used in this study. The same viscometer was used to measure the oil viscosity at various temperatures and atmospheric pressure and the results are depicted in Figure 2.

Table 3. Physical properties of the light crude oil sample used in this study at P_{atm} = 101.1 kPa and T_{exp} = 25 °C.

Property	Value
Molecular weight	223 gr/mol
Density at 101.1 kPa & 25 °C	799 kg/m^3
Viscosity at 101.1 kPa & 25 °C	2.76 mPa.s
n-C_5 insoluble asphaltene content	1.23 wt.%

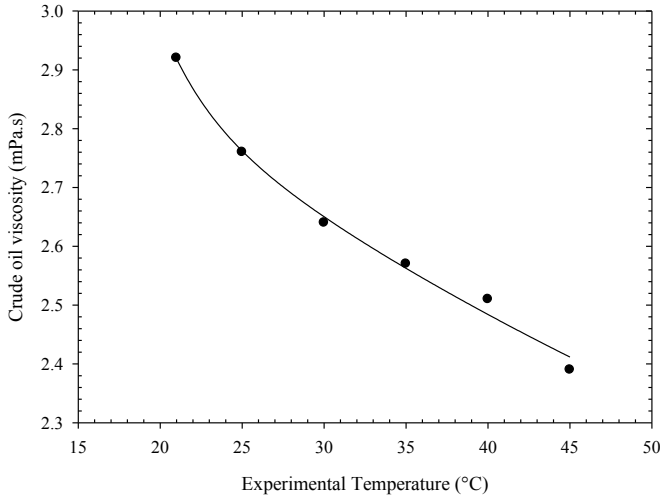

Figure 2. Measured values of crude oil viscosity as a change of experimental temperature at atmospheric pressure (i.e., P_{atm} = 101.1 kPa).

3. CO_2–brine system

3.1. CO_2 solubility measurement in brine

The apparatus used for measuring CO_2 solubility in brine was mainly composed of a CO_2 cylinder, a programmable syringe pump (Teledyne ISCO, 500D series), an air bath with a heater and temperature controller, a digital pressure gauge (Heise Inc.), a piston accumulator, a back pressure regulator (BPR) with maximum operating pressure of P_{max} = 34.5 MPa (Temco Inc.), and effluent fluid (CO_2 and water) collectors. The detailed schematic diagram of the solubility measurement setup utilized to determine CO_2 solubility in brine is depicted in Figure 3. The accuracy of the pressure gauges and temperature controller were ±0.7 kPa in the pressure range of 0–34.5 MPa and ±0.1 °C in the temperature range of 0–100 °C, respectively.

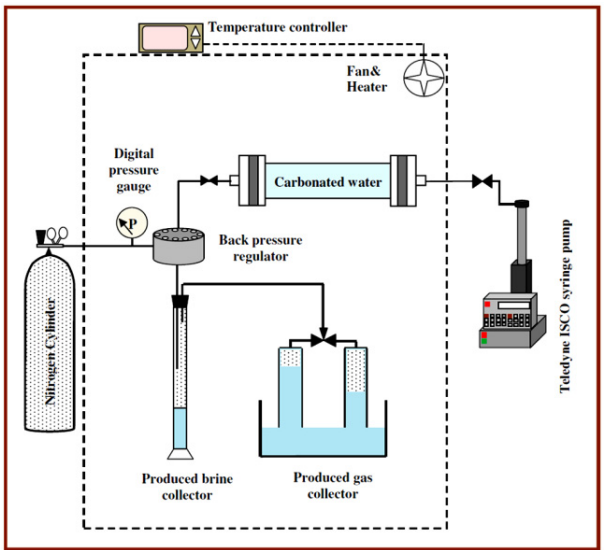

Figure 3. Schematic diagram of the experimental setup used to measure CO_2 solubility in brine at various equilibrium pressures and constant temperature of T_{exp} = 25 °C.

The process of mixing CO_2 with brine was conducted at pre-determined experimental temperature and pressure. CO_2 was injected from a high pressure cylinder into the piston accumulator which contains synthetic brine. The mixture was homogenized for 48 hours inside the airbath set at experimental temperature while the outlet pressure of the CO_2 cylinder was kept constant. During the equilibration process, the cylinder was kept connected to CO_2 cylinder in order to provide the pressure support on the mixture. Then the mixture was oriented vertically and connected to the BPR set at the same pressure to release the free gas remained on the top of the CO_2-saturated brine. The mixture was pushed upward by injecting hydraulic oil from the bottom side of piston accumulator until the water comes out from the BPR, indicating that the free CO_2 was removed and the CO_2–brine mixture is in saturated liquid phase.

When the CO_2-saturated brine was prepared and stabilized, a subsample was taken out through BPR. Eventually, by measuring the volumes of the produced CO_2 and brine in collectors, gas to water ratio (GWR) was calculated to determine the CO_2 solubility in brine, as given in Equations 1 and 2.

$$GWR = \frac{Produced\,CO_2, cm^3\left(P_{atm}, T_{\exp}\right)}{Produced\,Water, cm^3\left(P_{atm}, T_{\exp}\right)} \tag{1}$$

$$\chi_b = GWR \times \frac{\rho_{CO_2}}{\rho_b} \times \frac{1000}{MW_{CO_2}} \tag{2}$$

3.2. CO_2 solubility in brine

In this study, the solubility of CO_2 in brine with the salinity of s = 0.3492 mole NaCl/kg water at different equilibrium pressures and four constant temperatures ranging T_{exp} = 21–40 °C was determined. Figure 4 depicts the measured values of CO_2 solubility in brine at various equilibrium pressures. Results show that the CO_2 solubility in brine increases remarkably with equilibrium pressure up to a certain point. Further increase in equilibrium pressure beyond this point did not result in noticeable increase in CO_2 solubility in brine. This behaviour is mainly due to the CO_2 phase change from gas to liquid which occurs near CO_2 liquefaction pressure, P_{liq}. In the other hand, since the molecular diffusion is the main mechanisms leading to CO_2 dissolution, and also the diffusion coefficient of gaseous CO_2 in brine is significantly higher than that of liquid CO_2, further dissolution of CO_2 in brine is very limited at pressures higher than the CO_2 liquefaction pressure. As it can be seen in Figure 4, the experimental data of CO_2 solubility in brine is also in a fair agreement with those predicted using the model developed by Duan *et al.* [26]. However, one may consider that even small differences in CO_2 solubility values might results in significant consequences when a field scenario is considered.

CO_2 solubility in pure water was also measured at equilibrium pressure of P_{eq} = 4.1 MPa and various experimental temperatures of T_{exp} = 21–40 °C in order to determine the salinity effect on CO_2 solubility and the results are compared in Figure 5. It was found that at each constant temperature, the solubility of CO_2 is reduced by adding NaCl to the pure water. For instance at temperature of T_{exp} = 25 °C, solubility of CO_2 was dropped from χ_w = 1.1029 mole/kg in pure water to χ_b = 0.9738 mole/kg in 2 wt.% NaCl brine. This is mainly due to the fact that the solubility of CO_2 in aqueous solutions usually decreases after adding inorganic salts. When the NaCl concentration is increased, some of the water molecules are attracted by the Na^+ and Cl^- ions, which decreases the number of water molecules available to interact with CO_2. This phenomenon is called the salting-out effect [18].

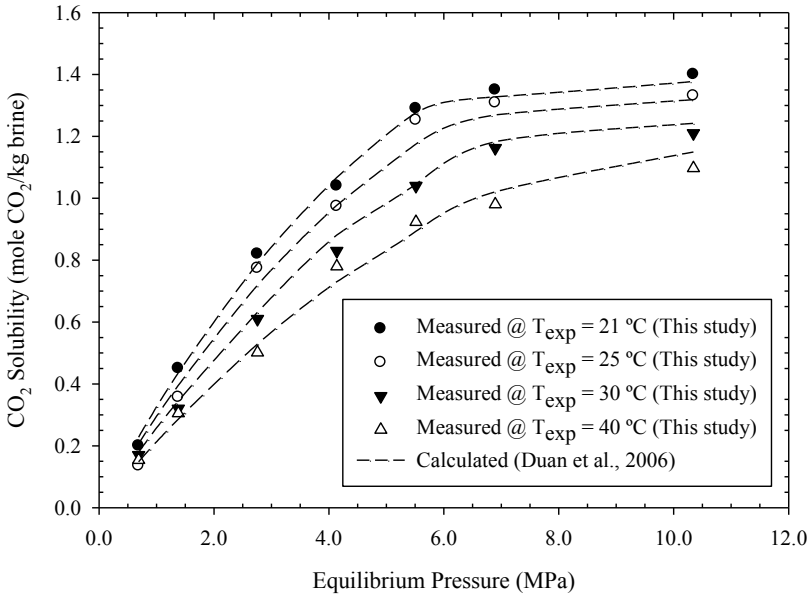

Figure 4. Comparison of measured and calculated CO_2 solubility in brine at various equilibrium pressures and experimental temperatures.

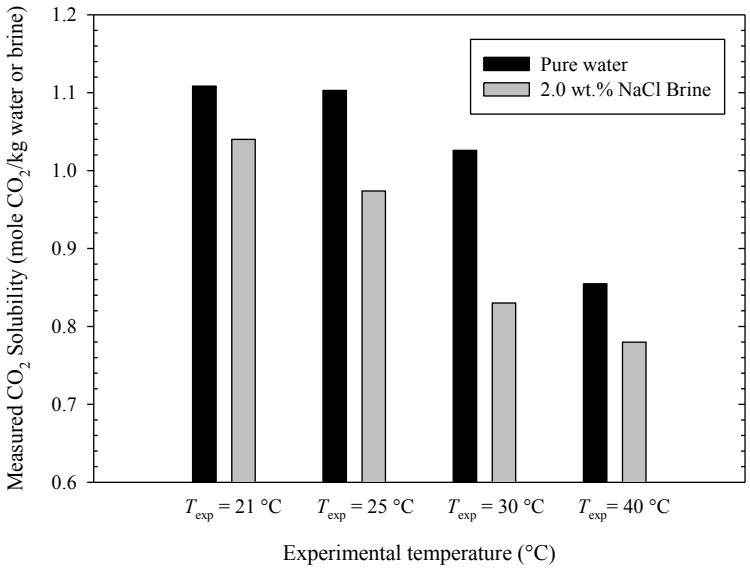

Figure 5. CO_2 Solubility in pure water and 2.0 wt.% brine samples at equilibrium pressure of P_{eq} = 4.1 MPa and various experimental temperatures.

4. CO_2–Oil system

4.1. CO_2 solubility measurement and oil swelling/extraction tests

Figure 6 shows the schematic diagram of the experimental apparatus for measuring the CO_2 solubility in the crude oil. The apparatus mainly consisted of a high pressure–high temperature visual cell (Jerguson Co.), a magnetic stirrer (Fisher Scientific Co.) and a high pressure CO_2 cylinder. The setup was placed in an airbath so that constant temperature is maintained using a temperature controller (Love Controls Co.) during the solubility measurement tests. The magnetic stirrer was placed underneath the visual cell in which the crude oil sample and a magnet bar were placed in. The oil sample rotation greatly accelerated the CO_2 dissolution into the crude oil by creating convective mass transfer [29–30]. The pressure inside the pressure cell was also measured by using a digital pressure gauge (Heise Inc.).

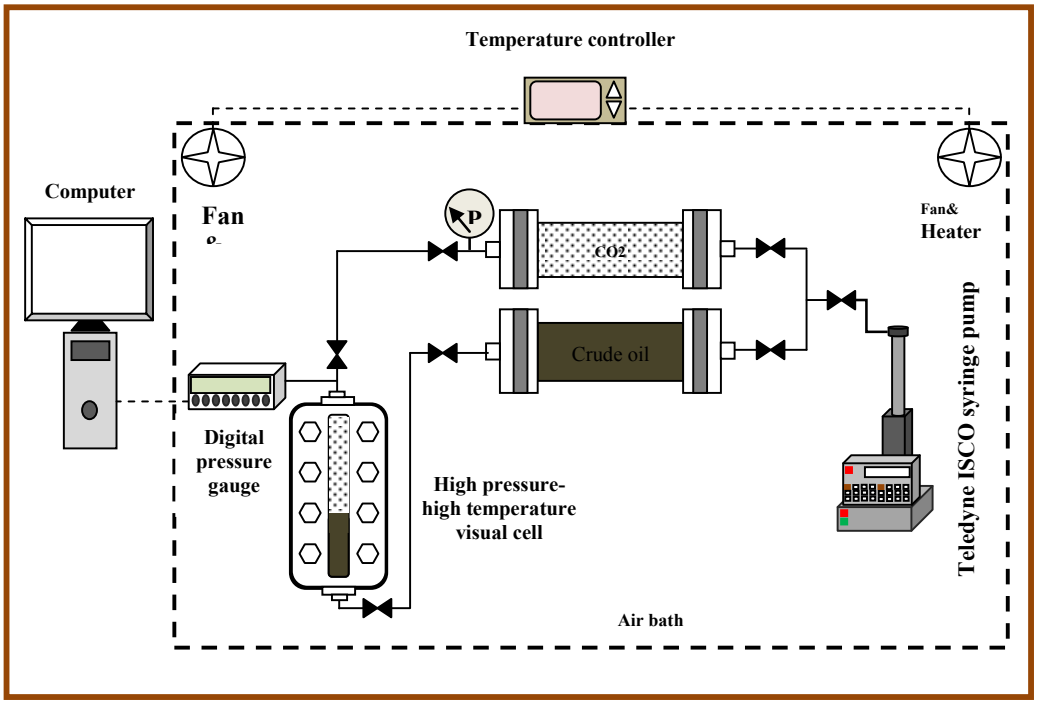

Figure 6. Schematic diagram of the experimental setup used for measuring the CO_2 solubility for CO_2–oil systems at various pressures and a constant experimental temperature.

The CO_2 solubility in crude oil was measured at different equilibrium pressures and four constant temperatures in the range of T_{exp} = 21–40 °C. The temperature of the airbath was set at desired value, T_{exp}, prior to each solubility measurement. The high-pressure cell was charged with $V_{o,i}$ = 25 cm^3 of the crude oil sample. Then the pressure cell was pressurized with CO_2 to a pre-specified pressure, P_i. The pressure of the cell was allowed to stabilize while CO_2 was dissolving into the crude oil. The test was terminated when the pressure inside the cell reached its stable value and no more pressure drop was observed ($\Delta P \leq 0.7$ kPa/day), i.e. the final CO_2 pressure, P_f. Finally, initial and final volumes of CO_2 in visual cell, $V_{CO2,i}$ and $V_{CO2,f}$, respectively, were determined by taking photos and utilizing image analysis technique. Throughout this study, the solubility was defined as the ratio of the total mass of dissolved CO_2 in 100 gr of the original crude oil sample. It was calculated using the mass balance and ideal gas equations for the dissolution process. Detailed derivation of CO_2 solubility formulations is as follow:

$$
\begin{aligned}
m_{dis} &= m_{CO_2,i} - m_{CO_2,f} \\
&= \left(\frac{PV_{CO_2}M_{CO_2}}{ZRT}\right)_i - \left(\frac{PV_{CO_2}M_{CO_2}}{ZRT}\right)_f \\
&= \frac{M_{CO_2}}{RT_{\exp}}\left[\left(\frac{PV_{CO_2}}{Z}\right)_i - \left(\frac{PV_{CO_2}}{Z}\right)_f\right]
\end{aligned}
\tag{3}
$$

$$
m_{oil} = \left(\rho_{oil}V_{o,i}\right)_{@T_{\exp}} \tag{4}
$$

$$
\begin{aligned}
\chi_{CO_2} &= \frac{m_{dis}}{m_{oil}} \times 100 \\
&= \frac{M_{CO_2}}{RT\rho_{oil}V_{o,i}}\left[\left(\frac{PV_{CO_2}}{Z}\right)_i - \left(\frac{PV_{CO_2}}{Z}\right)_f\right]
\end{aligned}
\tag{5}
$$

The swelling factor, *SF,* is determined by measuring the final volume of the crude oil in the cell, $V_{o,f}$, as a result of two mechanisms: CO_2 dissolution in the oil, and light to medium hydrocarbon groups extraction from the oil to the CO_2 phase. The swelling factor (*SF*) is expressed as the ratio of final CO_2-saturated oil volume, $V_{o,f}$, at experimental pressure and temperature divided by the original oil volume, $V_{o,i}$, at experimental temperature and atmospheric pressure.

$$
SF = \frac{V_{o,f}\left(P_{\exp}, T_{\exp}\right)}{V_{o,i}\left(P_{atm}, T_{\exp}\right)} \tag{6}
$$

4.2. CO_2 solubility in the oil phase

The CO_2 solubility in the crude oil was measured at various equilibrium pressures and four temperatures. The measured values of CO_2 solubility in the crude oil versus equilibrium pressure at different experimental temperatures is shown in Figure 7. It can be observed that the measured CO_2 solubility in the crude oil sample increases with the equilibrium pressure. Literally, the concentration of dissolved CO_2 depends on the partial pressure of the CO_2. If the partial pressure increases (i.e., higher equilibrium pressure), the number of CO_2 molecules collisions with the surface increases. As a result, higher CO_2 solubility in oil is obtained at higher equilibrium pressures. Moreover, it was seen that increasing the temperature leads to a reduction in the solubility of CO_2 in the crude oil. For example, at equilibrium pressures close to P_{eq} = 5.8 MPa, the solubility of CO_2 reduces from χ_b = 29.95 gr CO_2/100 gr Oil to χ_b = 21.65 gr CO_2/100 gr Oil when experimental temperature decreases from T_{exp} = 25 °C to T_{exp} = 40 °C. The measured CO_2 solubility values in crude oil were also calculated by using a correlation developed by Emera and Sarma [28] which were found to be more accurate compared to other correlations available in the literature [31]. The correlation is based on genetic algorithm and is a function of the saturation pressure, temperature, oil specific gravity, and oil molecular weight.

Figure 7 also illustrates the comparison of the experimental values of CO_2 solubility with those calculated by Emera and Sarma's correlation. It was found that the calculated CO_2 solubility data is in a fair agreement with the measured values within the range of the experimental conditions of this study.

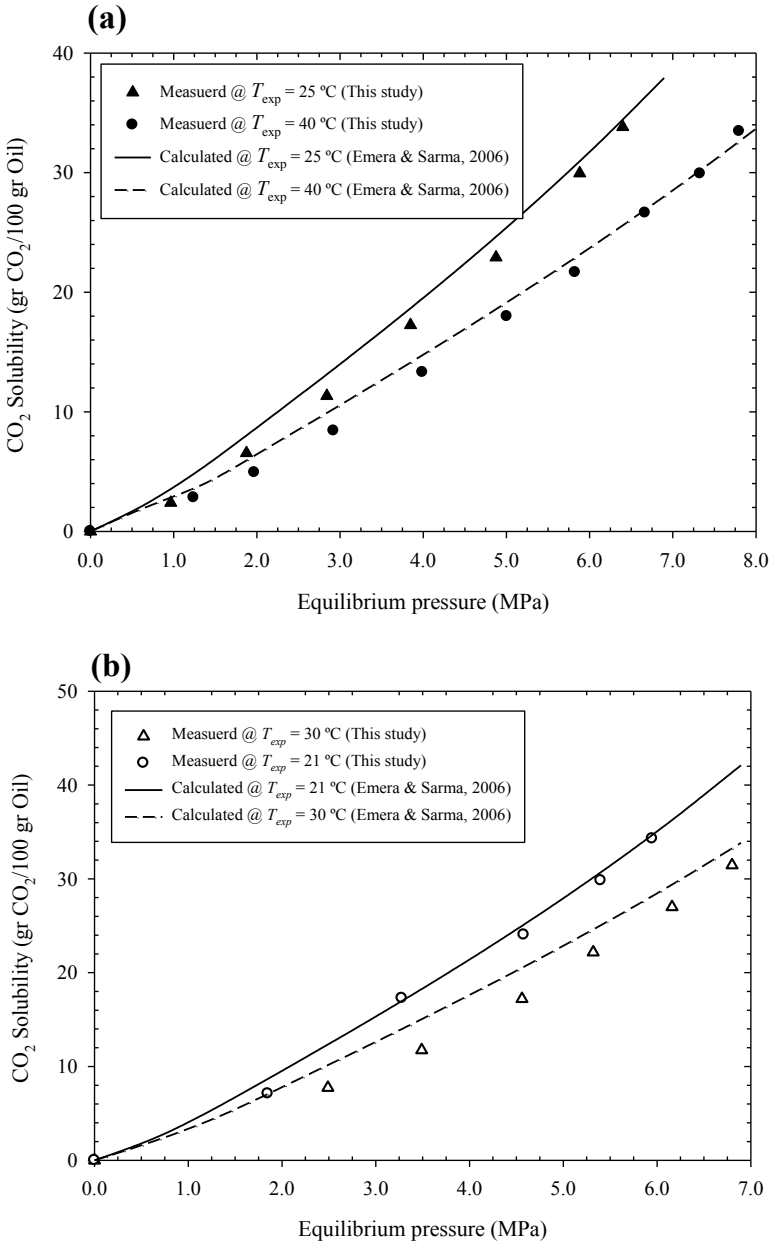

Figure 7. Measured and calculated CO_2 solubility in crude oil sample at different equilibrium pressures and two constant temperatures: (a) T_{exp} = 25 °C and 40 °C, and (b) T_{exp} = 21 °C and 30 °C.

4.3. Oil swelling factor and extraction pressure

Figure 8 depicts the oil swelling factor, *SF*, as a result of CO_2 dissolution in the oil phase at experimental temperatures in the range of T_{exp} = 21 to 40 °C. The oil swelling factor was equal to one at atmospheric pressure and experimental temperature. Afterward, by increasing the equilibrium pressure, the oil phase swelled and the oil swelling factor gradually became greater than one mainly due to higher solubility of CO_2 in the crude oil. As an

example, at experimental temperature of T_{exp} = 25 °C, maximum swelling occurred at the pressure of 6.4 MPa, at which maximum swelling factor and CO_2 solubility of SF = 1.3571 and $\chi_{o,max}$ = 33.11 gr CO_2/100 gr Oil were achieved, respectively. It was also found that during the swelling/extraction tests, the oil swelling factor curves exhibits a sharp decline at a certain pressure which is known as extraction pressure, P_{ext}. At this pressure, majority of light to medium hydrocarbon groups of the crude oil were extracted by CO_2 and vaporized into the CO_2-rich phase. Maximum CO_2 solubility, $\chi_{o,max}$, maximum oil swelling factor, SF_{max}, and extraction pressure, P_{ext}, obtained at various operating temperatures are summarized in Table 4. At equilibrium pressures beyond the extraction pressure, the CO_2–oil interaction is majorly governed by extraction of the remaining light to medium hydrocarbon rather than the oil swelling. Thus, the oil phase started to shrink and the oil swelling factor was reduced. The oil swelling factor reduction was observed to be continuous as the equilibrium pressure was further increased. This can be attributed to the formation of high-density CO_2-rich phase which has higher capability to extract light to medium hydrocarbon components of the crude oil [32–33]. The impact of experimental temperature on swelling/extraction curve is also presented in Table 4 and the results revealed that the maximum swelling factor decreases with increased experimental temperatures. In addition, the extraction pressures of the CO_2–oil system are greater at higher temperatures compared to those at lower ones. As an example, the extraction pressure of P_{ext} = 6.8 MPa at T_{exp} = 30 °C reduced to P_{ext} = 6.0 MPa at T_{exp} = 21 °C.

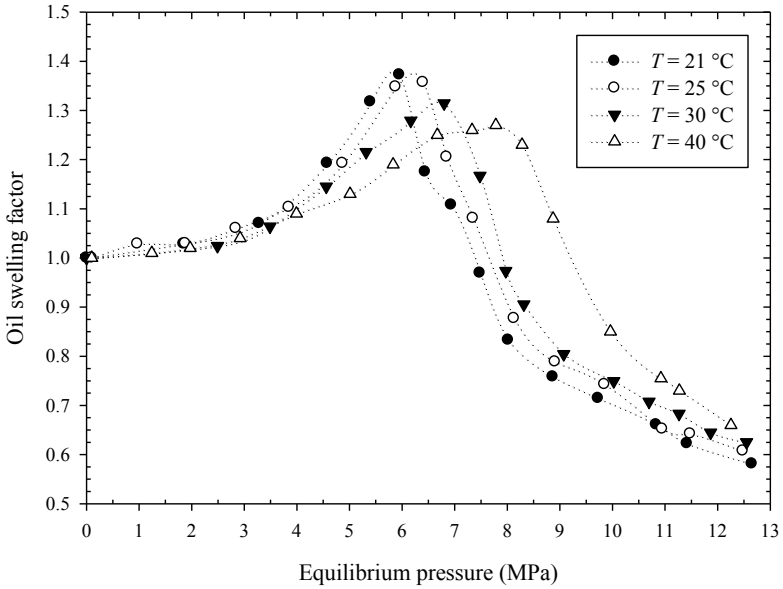

Figure 8. Measured oil swelling factor of crude oil–CO_2 system versus equilibrium pressure at various experimental temperatures.

Table 4. Measured extraction pressure, maximum CO_2 solubility, and oil swelling factor for swelling/extraction tests conducted at various experimental temperatures.

Experimental Temperature, T_{exp} (°C)	Measured extraction pressure, P_{ext} (MPa)	Maximum CO_2 solubility, $\chi_{o,max}$ (grCO_2/100grOil)	Maximum oil swelling factor, SF_{max}
21	6.0	33.8	1.37
25	6.4	34.2	1.36
30	6.8	31.4	1.31
40	7.8	33.45	1.27

Figure 9 also illustrates the CO_2 solubility along with the swelling factor for CO_2–oil system at various equilibrium pressures and experimental temperatures of T_{exp} = 21 to 40 °C. As it can be observed, the solubility of CO_2 in oil sample and the oil swelling factor increase noticeably as the pressure increases up to the extraction

pressure, P_{ext}. This figure obviously depicts that there is a direct relationship between the CO_2 solubility in the crude oil sample and the oil swelling factor. For the pressures higher than P_{ext}, light to medium hydrocarbon groups extraction is a dominant process and the chemical composition of both liquid and vapour phases change frequently.

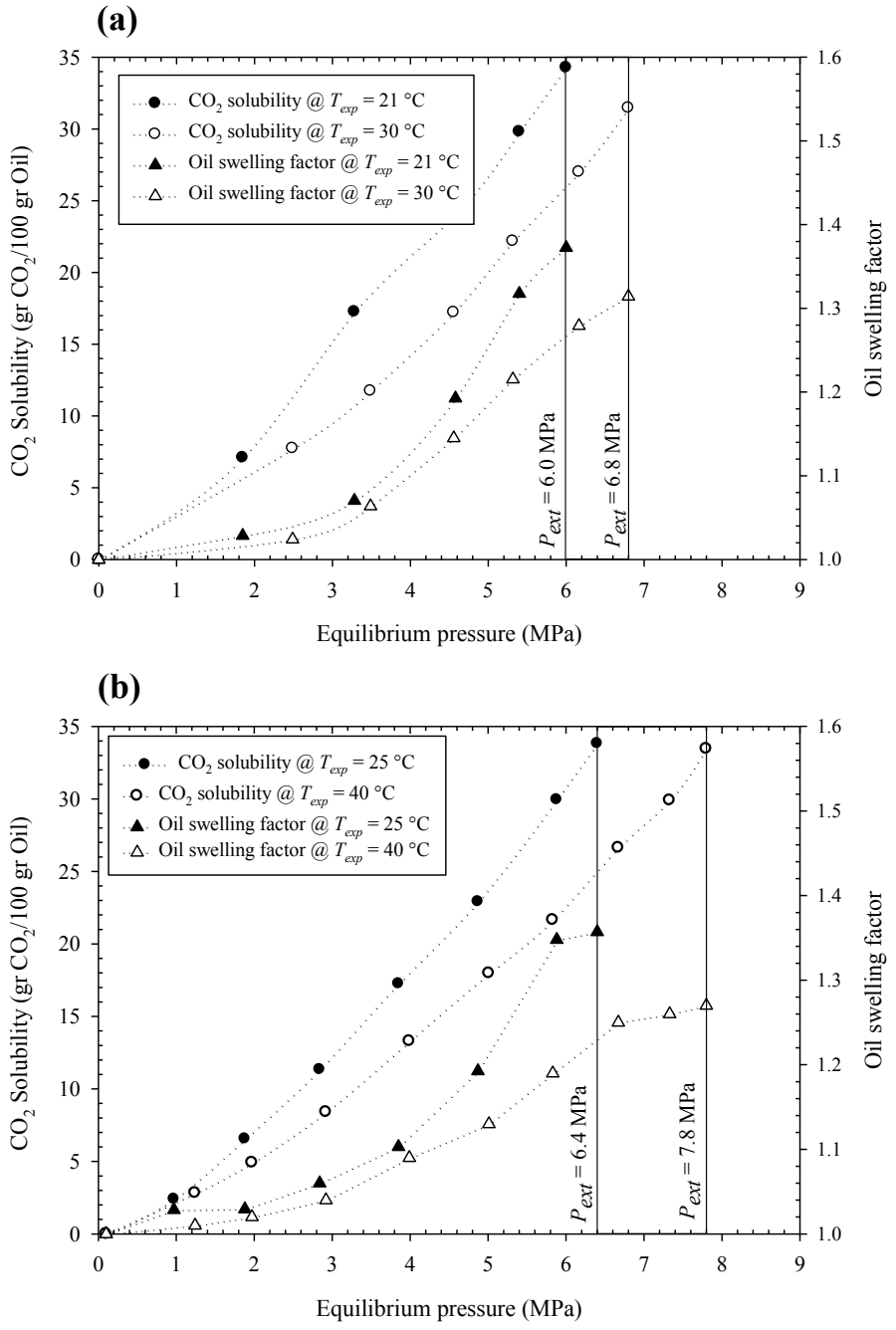

Figure 9. CO_2 solubility in crude oil and oil swelling factor at various operating pressure and four constant temperatures: (a) T_{exp} = 21 °C and 30 °C and (b) T_{exp} = 25 °C and 40 °C.

The maximum CO_2 solubility values in oil which were existed at extraction pressure for different swelling/extraction tests conducted at different experimental temperatures are indicated in Figure 10. The results showed that the maximum CO_2 solubility values which are required to initiate the extraction of major light to medium hydrocarbon groups are approximately the same for different experimental temperatures. Therefore, it can be concluded that light to medium hydrocarbon extraction occurs when a definite amount of CO_2 is dissolved into the oil which is called threshold CO_2 solubility, χ_{th}. The threshold CO_2 solubility for the CO_2–oil system of this study was found to be χ_{th} = 33.21 gr CO_2/100 gr Oil. Figure 11 depicts the extraction pressures of CO_2–Oil system at different experimental temperatures. Since CO_2 solubility in oil is directly proportional to equilibrium pressure while inversely proportional to experimental temperature, higher pressure is required to reach the threshold CO_2 solubility as the experimental temperature increases. Therefore, higher extraction pressure was observed at higher experimental temperatures. The threshold CO_2 solubility parameter defined in this study has a unique value for each CO_2–oil mixture depending on the composition of the crude oil. For a particular crude oil composition saturated with CO_2, this parameter can be used to estimate the extraction pressure at various temperatures. Moreover, the experimental data obtained for the extraction pressure showed a linear behaviour with experimental temperature as indicated in Figure 11. The extraction pressure was observed to increase linearly from P_{ext} = 6.0 MPa at T_{exp} = 21°C to P_{ext} = 7.8 MPa at T_{exp} = 40°C.

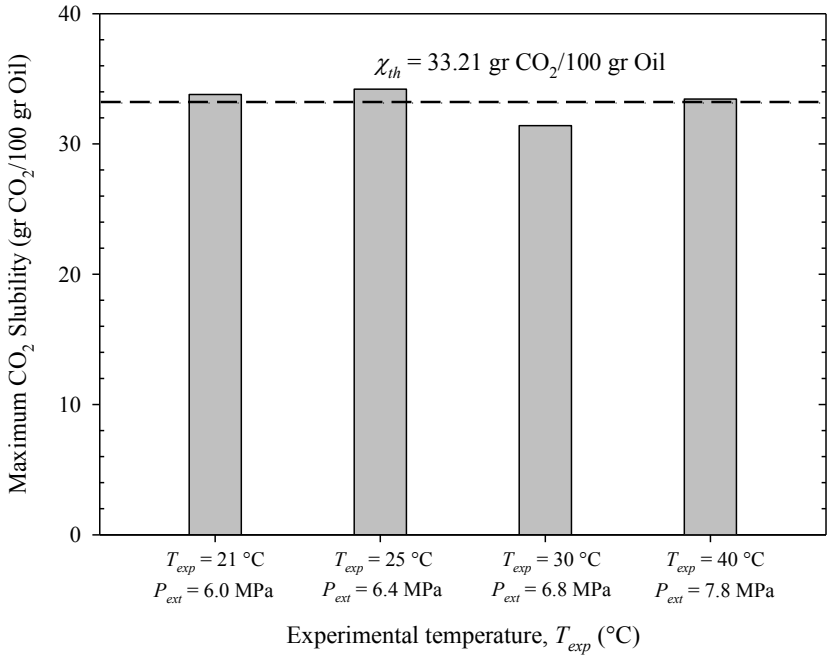

Figure 10. Threshold CO_2 solubility values and extraction pressures for different experimental temperatures.

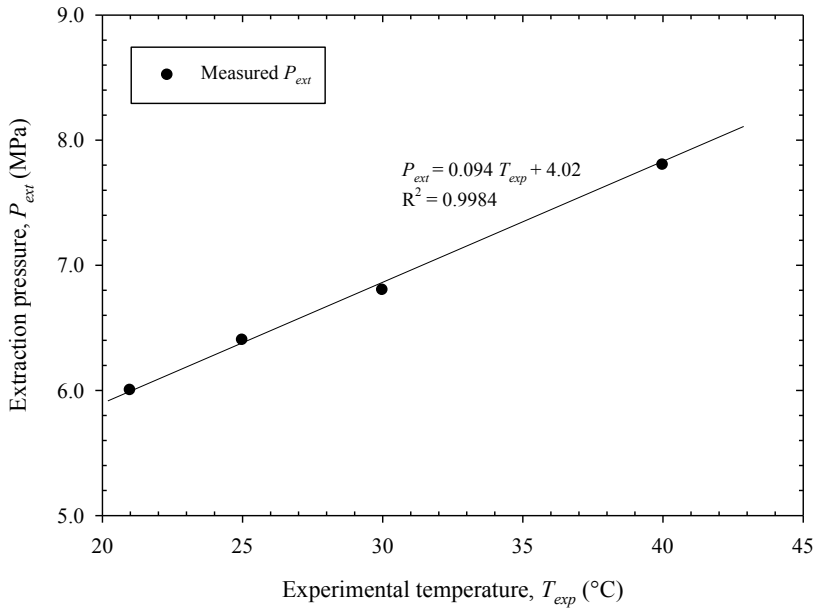

Figure 11. Measured extraction pressure, P_{ext}, for the CO_2–oil system at various experimental temperatures and the linear equation fitted to the experimental data points.

5. Conclusions

A detailed phase behaviour study on the CO_2–water, CO_2–brine, and CO_2–oil systems was conducted through carefully-designed laboratory experiments. CO_2 solubility measurements in water, brine, and oil phases were conducted at various experimental conditions. Afterward, swelling/extraction tests were carried out for CO_2–oil system to examine the oil swelling and light component extraction during various equilibrium pressures in the range of P_{eq} = 0.7–10.3 MPa and experimental temperatures in the range of T_{exp} = 21–40 °C. It is believed that the findings of this study are critical to any CO_2 EOR and storage projects. The main conclusions of this study are summarized as follows:

- The solubility of CO_2 in brine increases with increased pressure at constant temperature and salinity. In addition, the impact of pressure on CO_2 solubility diminishes as the pressure of the system increases. Moreover, the solubility of CO_2 in brine decreases at higher temperatures. The comparison of the CO_2 solubility in pure water and synthetic brine (2.0 wt.% NaCl) also indicated that the addition of salt leads to a reduction in CO_2 solubility in water.

- The CO_2 solubility in the oil phase is directly proportional to pressure while inversely proportional to the operating temperature. The CO_2 solubility increases steadily with pressure at any constant experimental temperatures. However, the growth is noticeably higher for the solubility measurement tests carried out at lower experimental temperatures.

- At a constant temperature, the swelling factor increases with pressure until extraction pressure, P_{ext}, at which most of the light to medium hydrocarbon groups of the oil are extracted and vaporized into the CO_2-rich phase. For the pressures higher than extraction pressure, the oil shrinks and the oil swelling factor decreases substantially. Furthermore, the maximum oil swelling factor is higher for swelling/extraction tests conducted at lower temperatures.

- Existence of threshold CO_2 solubility, χ_{th}, in the oil phase is the necessary and sufficient condition for the extraction of major light to medium hydrocarbon groups. This threshold CO_2 solubility was approximately χ_{th} = 33.21 gr CO_2/100 gr Oil for the oil sample under this study. In addition, the threshold CO_2 solubility was found to be independent of temperature and was the same for all swelling/extraction tests performed at different experimental temperatures.

Acknowledgment

The authors wish to acknowledge the funding support from Sustainable Technologies for Energy Production Systems (STEPS), Business-Led Network of Centres of Excellence (BL-NCE), Petroleum Technology Research Centre (PTRC), and Faculty of Graduate Studies and Research (FGSR) at the University of Regina.

References

[1] N. Mosavat, F. Torabi, Ind. Eng. Chem. Res. 53 (3) (2014) 1262–1273.
[2] A. Abedini, F. Torabi, Ind. Eng. Chem. Res. 52 (43) (2013) 15211–15223.
[3] F.M. Orr, J.P. Heller, J.J. Taber, J. Am. Oil Chem. Soc. 59 (10) (1982) 810A–817A.
[4] L. Nghiem, V. Shrivastava, B. Kohse, M. Hassam, C. Yang, Canadian International Petroleum Conference, Calgary, Alberta, June 16–18, 2009, Paper 2009–156.
[5] E. Lindeberg, D. Wessel-Berg, Energy Convers. Manage. 38 (1997) 229–234.
[6] J. Ennis-King, L. Paterson, SPE J. 10 (3) (2005) 349–356.
[7] R. Simon, D.J. Graue, Journal of Petroleum Technology, 17 (1965) 102–106.
[8] A.K.M. Jamaluddin, N.E. Kalogerakis, A. Chakma, Fluid Phase Equilib. 64 (1991) 33–48.
[9] R.K. Srivastava, S.S. Huang, S.B. Dyer, F.M. Mourits, 6th UNITAR International Conference on Heavy Crude and Tar Sands, Houston, Texas, February 12–17, 1995.
[10] G.M.N. Costa, P.S.M.V. Rocha, A.L.C. Riberio, P.R.F. Menezes, R.C.A. Lima, P.U.O. Costa, E.A. Rodrigues, J. Petrol. Sci. Eng. 98 (2012) 144–155.
[11] A. Abedini, F. Torabi, Energy Fuels. DOI: 10.1021/ef401363b.
[12] R.M. Enick, S.M. Klara, Chem. Eng. Commun. 90 (1) (1990) 23–33.
[13] A. Bamberger, G. Sieder, G. Maurer, J. Supercrit. Fluids, 17 (2000) 97–110.
[14] A.N. Sabirzyanov, R.A. Shagiakhmetov, F.R. Gabitov, A.A. Tarzimanov, F.M. Gumerov, Theor. Found. Chem. Eng. 37(1) (2003) 51–53.
[15] A. Chapoy, A.H. Mohammadi, A. Chareton, B. Tohidi, D. Richon, Ind. Eng. Chem. Res. 43 (7) (2004) 1794–1802.
[16] A. Valtz, A. Chapoy, C. Coquelet, P. Paricaud, D. Richon, Fluid Phase Equilib. 226 (2004) 333–344.
[17] J.M. Han, H.Y. Shin, B.-M. Min, K.-H. Han, A. Cho, Ind. Eng. Chem. Res. 15(2) (2009) 212–216.
[18] Y. Liu, M. Hou, G. Yang, B. Han, J. Supercrit. Fluids, 56 (2) (2011) 125–129.
[19] D. Koschel, J.-Y. Coxam, L. Rodier, V. Majer, Fluid Phase Equilib. 247 (1-2) (2006) 107–120.
[20] J. Kiepe, S. Horstmann, K. Fischer, G. Gmehling, Ind. Eng. Chem. Res. 41 (2002) 4393–4398.
[21] F. Gu, Journal of Chemical Engineering of Chinese Universities, 12(2) (1998) 118–1231.
[22] B. Rumpf, H. Nicolaisen, C. Ocal, G. Maurer, J. Solution Chem. 23 (1994) 431–448.
[23] L.W. Diamond, N.N. Akinfiev, Fluid Phase Equilib. 208(1–2) (2003) 265–290.
[24] I. Mohamed, J. He, H.A. Nase-El-Din, Journal of Petroleum Science Research, 2 (1) (2013) 14–26.
[25] Z. Duan, R. Sun, Chem. Geol. 193 (2003) 257–271.
[26] Z. Duan, R. Sun, C. Zhu, M. Chou, Mar. Chem. 98 (2) (2006) 131–139.
[27] S. Mao, D. Zhang, Y. Li, N. Liu, Chem. Geol. 347 (2013) 43–58.
[28] M.K. Emera, H.K. Sarma, Canadian International Petroleum Conference, Calgary, Alberta, June 13–15, 2006, Paper SPE 2006-197.
[29] A. Abedini, F. Torabi, N. Mosavat, Journal of Mathematics and System Science, 2 (2012) 409–419.
[30] A. Kavousi, F. Torabi, C. Chan, SPE Heavy Oil Conference Canada, Calgary, Alberta, June 11–13, 2013, Paper SPE 165559.
[31] M. Al-Jabra, B.D. Al-Anazi, NAFTA, 60 (5) (2009) 287–291.
[32] J.S. Tsau, L.H. Bui, G.P. Willhite, SPE Improved Oil Recovery Symposium, Tulsa, Oklahoma, April 24–28, 2010, SPE Paper 129728-MS.
[33] L.H. Bui, J.S. Tsau, G.P. Willhite, SPE Improved Oil Recovery Symposium, Tulsa, Oklahoma, April 24–28, 2010, SPE Paper 129710-MS.